One-shot fault diagnosis of 3D printers through improved feature space learning

Chuan Li, *Senior Member, IEEE*, Diego Cabrera, Fernando Sancho, René-Vinicio Sánchez, Mariela Cerrada, José Valente de Oliveira

***Abstract*—Signal acquisition from mechanical systems working in faulty conditions is normally expensive. As a consequence, supervised learning-based approaches are hardly applicable. To address this problem, a one-shot learning-based approach is proposed for multi-class classification of signals coming from a feature space created only from healthy condition signals and one single sample for each faulty class. First, a transformation mapping between the input signal space and a feature space is learned through a bidirectional generative adversarial network. Next, the identification of different health condition regions in this feature space is carried out by means of a single input signal per fault. The method is applied to three fault diagnosis problems of a 3D printer and outperforms other methods in the literature.**

***Index Terms*—Deep learning, Fault diagnosis, One-shot learning, 3D printer.**

I. Introduction

THE use of additive manufacturing technologies, i.e., the process of making 3D objects by adding layer upon layer of raw material, has increased significantly i n r ecent years [1]. This popularity is mainly due to the time saved in the prototyping processes, as well as the technology's flexibility to be applied in almost all manufacturing areas [2], [3].

The quality of manufactured products is highly dependent on the machine's (viz. 3D printer) health condition [4], and therefore early fault diagnosis of the machine is a fundamental task.

This work was sponsored in part by GIDTEC Research Group of Universidad Politecnica Salesiana, the National Natural Science Foundation of China (51775112), the MoST Science and Technology Partnership Program (KY201802006), the Chongqing Natural Science Foundation (cstc2019jcyj-zdxmX0013), and the CTBU Project (KFJJ2018107, KFJJ2018075). (Chuan Li and Diego Cabrera are co-first authors.)(Corresponding author: Diego Cabrera.)

C. Li is with the National Research Base of Intelligent Manufacturing Service, Chongqing Technology and Business University, Chongqing 400067, China (e-mail:chuanli@21cn.com).

D. Cabrera is with the National Research Base of Intelligent Manufacturing Service, Chongqing Technology and Business University, Chongqing 400067, China, and the GIDTEC Group, Universidad Politécnica Salesiana, Cuenca 010102, Ecuador (tel:+59374056951, e-mail:dcabrera@ups.edu.ec).

F. Sancho is with the Department of Computer Science and Artificial Intelligence, Seville University, Seville 41012, Spain (e-mail: fsancho@us.es).

R. Sánchez and M. Cerrada are with the GIDTEC Group, Universidad Politécnica Salesiana, Cuenca 010102, Ecuador (e-mail: rsanchezl@ups.edu.ec; mcerrada@ups.edu.ec).

J.V. de Oliveira is with the Universidade do Algarve, Algarve 8005 139, Portugal (e-mail: jvo@ualg.pt).

Currently, machine learning-based methods are becoming the preferred design methods for machinery fault diagnosis, including fault diagnosis in 3D printers [5]. The general design methodology includes different types of signal acquisition [6]–[9], signal processing-based feature extraction [10]–[12], feature selection, and fault diagnoser synthesis (see [13], [14] for a survey on these topics with an emphasis on fuzzy formalisms). Feature extraction and selection are very challenging phases because an inappropriate feature space for classification may lead to poor classification performance. [15] uses the wavelet packet transform for feature extraction together with random forest classifiers for fault diagnosis of spur gears. In an extension of this work, [16] propose feature selection by introducing genetic algorithms into a wrapper strategy. In [17], a filtering-based approach for feature extraction is applied to additive manufacturing fault diagnosis. Moreover, [18] and [19] develop unsupervised approaches for feature selection based on Rough Set Theory with application in the fault diagnosis of rotating machinery.

The use of deep learning techniques in fault diagnosis in [20] permits feature extraction, selection, and fault classification in a single phase. Similarly, [21] uses a Sparse AutoEncoder (SAE) network for 3D printer fault diagnosis, [22] presents a Deep Convolutional AutoEncoder (DCAE) for automatic feature extraction in helical gears, [23] proposes a Convolutional Deep Belief Network (CDBN) for electric locomotive bearing fault diagnosis, and [24] introduces a transfer learning SVM-based approach. While these works exhibit competitive performances in their application, all of them explicitly or implicitly assume that enough data are available for every machine's health condition. However, from the signal acquisition perspective, such a situation — if even possible — is extremely expensive. Some works address this issue through unsupervised approaches. For example, [25] introduces the SAE-based sensor fusion for the 3D printer condition assessment, [26] combines an echo state network with a Variational AutoEncoder (ESN-VAE) for helical gearbox fault detection, and [27] uses a generative adversarial network (GAN) to capture the probability distribution of the healthy (no fault) condition. Meanwhile, [28] introduce the categorical GAN for condition clustering. None of these works require data availability in the sense mentioned above, but they only distinguish between the healthy and faulty conditions.

Another way to deal with the data availability issue is through the one-shot learning approach [29]. In this case, a model is trained to compare pairs of inputs instead of classify-

ing them. After training the model, only one example of a new class is required to classify a sample according to its similarity. The applicability of one-shot learning has been tested, for example, in human activity recognition [30], multitask traffic classification [31], a nd r obust m aterial c lassification [3 2]. In the field of fault diagnosis, it has been applied to fault classification of rolling bearings with limited data [33]. Although data requirements are reduced, its applicability is limited because it needs pairs of examples in different conditions in the training stage. To the best of our knowledge, no work has been reported addressing realistic data acquisition restrictions (rich in data from healthy conditions but little or no data from faulty conditions) to properly conduct feature extraction, selection, and fault diagnosis under semi-supervised or unsupervised frameworks.

In this work, we propose a one-shot learning method for fault diagnosis in 3D printers. The contributions of this work include the following: (i) an unsupervised learning procedure based on bidirectional generative adversarial networks (BiGANs) to map the signal input space into a feature space suitable for classification, by using only signals acquired in the healthy condition; (ii) the definition o f r epresentative vectors (RVs) representing health condition regions adequate for fault diagnosis; (iii) a method to classify a signal into one of the health conditions in the feature space; and (iv) the application of the proposed method to three exemplar cases of fault diagnosis in 3D printers, including a comparison with existing feature extraction and feature classification methods.

The remainder of the paper is organized as follows. Section II describes the complete methodology proposed. Section III presents the case studies on 3D printer fault diagnosis. Finally, Section IV is dedicated to presenting some conclusions of the work.

II. Methodology

The core of the proposed method is to learn a mapping from the signal space to an adequate feature space in an unsupervised way. This mapping allows us to obtain vectors that represent health condition regions in the feature space and that are suitable for classification u nder s trict d ata availability requirements. Fault diagnosis is accomplished from these vectors as follows.

Let $\mathbf{v}$ be a vector in this feature space representing a certain health condition. Inputs from the same health condition will be represented by vectors close to $\mathbf{v}$. Under ideal mapping, different health conditions will occupy different and separable regions in the feature space, and consequently, unseen signals can be classified i nto t he s ame c lass a s t he n earest RV.

Since the goal is to provide an adequate feature space and mapping (and not the class), the only data required during training is a set of input signals from the same health condition. In the actual context of fault diagnosis, signals from the healthy operating condition are feasible and cost-effective as they are usually very easy to obtain.

Consequently, to accomplish the fault diagnosis task, the following 4-step method is proposed (Fig. 1):

1) Acquisition of input signals: in this step, signal acquisition from the healthy condition, and one signal from each faulty condition, are required as information sources for the subsequent steps;
2) Input-to-feature space mapping: by using unsupervised learning of a feature model based on BiGAN, a mapping from the original signal space to the feature space is established using only signals from the healthy condition;
3) One-shot learning: the mappings of each signal from each faulty condition are calculated and stored for later diagnosis of forthcoming unseen signals (representative vectors);
4) Fault diagnosis: new unseen signals are mapped into the feature space and classified according to their proximity to the existing representative vectors.

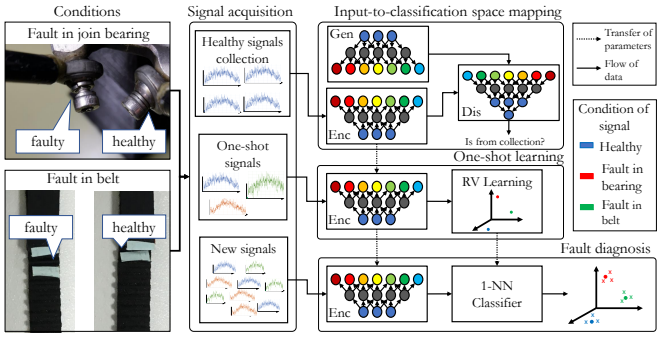

Fig. 1. Proposed methodology for one-shot learning fault diagnosis.

Details of these steps are presented below. In what follows, let us suppose that we are working with a machine that can operate in K possible conditions, $C = \{c_1, ..., c_K\}$, where c_1 will represent the only healthy condition. Let $s(t) \in \mathbb{R}^{T\times 1}$ be an input signal of large enough length, T, to capture signal dynamics. For a signal acquisition system operating for P seconds at a sampling frequency f_s (samples/seconds), the signal length will be $T = P \cdot f_s$.

A. Acquisition of input signals

In this step, a first set D_{health} of signals in condition c_1 is built. These signals are abundant and can be easily obtained. Additionally, a second set $D_{shot} = \{s_c(t) \mid c \neq c_1\}$, which contains one signal per faulty condition, is also acquired. Note that this last set is not required for training, and it can be obtained (as will most often be the case) incrementally whenever the machine manifests a particular fault throughout its useful life. This is in clear contrast with the classical fault classification approach, where a dataset with enough signals from every machine condition is required for training.

From a practical point of view, a new signal should be added to D_{shot} when an expert inspects the machine and finds a new previously unseen faulty condition. Although it is beyond the scope of this work to propose an approach to automatically determine new conditions, the ability to detect unseen fault conditions of the resulting model is discussed in Section III-D.

B. Input-to-feature space mapping

The space of signals, $\mathcal{S}$, that can be obtained from structurally non-trivial machinery operating conditions is highly

complex. Dealing directly with this space would result in a fruitless diagnosis. Therefore, it is often necessary to embed it into a more informative feature space (usually, a vector space of dimension d), $m : \mathcal{S} \rightarrow \mathcal{F}$.

For classification tasks such as fault diagnosis, we expect m to group vectors from the same class (machine condition), and separate different classes. Standard supervised deep learning techniques propose to find m by minimizing a loss function through a large number of training instances from all available classes.

However, to find m in an unsupervised way, we propose an idea based on the inverse transformation sampling technique [34]: if a known distribution is assigned to $\mathcal{F}$, then it is possible to find m^{-1} and improve m and m^{-1} simultaneously.

When approximating m and m^{-1} by neural networks, the input for m^{-1} comes from uniformly sampling a random vector of $\mathcal{F}$, while its output is in $\mathcal{S}$. Since these two networks are closely related, we can use the adversarial paradigm to consider an Encoder (Enc) for m, a Generator (Gen) for m^{-1}, and a Discriminator (Dis) network for optimizing all together. These three models together form a BiGAN model [35], whose optimization can be represented by the following minimax optimization problem over a loss function L:

$$\underset{\theta_{Gen},\theta_{Enc}}{\operatorname{argmin}} \ \underset{\theta_{Dis}}{\operatorname{argmax}} L(\theta_{Dis}, \theta_{Gen}, \theta_{Enc}) \tag{1}$$

where θ_{Dis}, θ_{Gen} and θ_{Enc} represent the parameters (weights) associated with the Dis, Gen, and Enc networks, respectively. The training procedure can be solved through a gradient-based optimization algorithm such as Adam [36].

To model Enc and Dis, we choose 1D convolutional neural networks (1DCNNs), and a 1D transpose convolutional neural network (1DTCNN, also called a deconvolutional neural network) for Gen, because these network architectures can directly deal with raw input signals (1DCNN) or generated signals (1DTCNN) that are characterized by the presence of cyclo-stationary patterns. Besides, the risk of over-fitting in convolutional-based models is lower than in a fully connected neural network because of the lower number of parameters in the former.

Since Gen and Enc will approximate inverse functions, we will take them with exactly symmetric architectures. Their number of layers and output channels in each layer are selected to minimize the amount of information loss during the transformations with an input length factor reduction of 2 (see Fig. 2). Furthermore, for the three neural networks, the batch normalization process described in [37] is applied to decrease the number of iterations for the convergence and directly deal with unnormalized inputs. However, this normalization is not applied to the last layer to avoid the variance increasing at the output. Additionally, the dimension matching in each layer is controlled by selecting the correct *padding* factor. For more information, refer to [38].

The specific network architectures used for the 3D printer fault diagnosis scenarios will be described in Section III-A.

C. One-shot learning

From the previous step, we obtain the Enc network optimized to transform input signals in the healthy condition to a neighbor region ($[-1, 1]^d$) of the origin of $\mathcal{F}$. Moreover, during Enc training, the orthogonality of the space is achieved with the optimization.

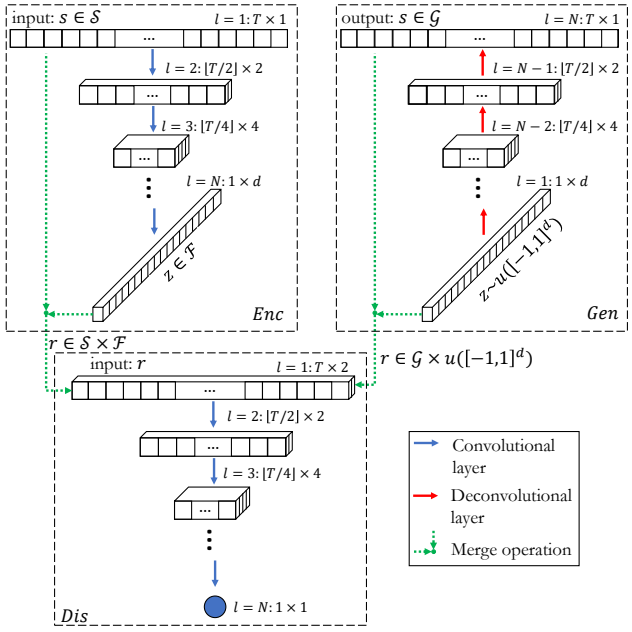

Fig. 2. Architecture of BiGAN. Each layer is described by its output length and channels; e.g., $T \times 2$ means 2 output channels of length T.

Additionally, we hypothesize that the restriction in the range of the mapping ($[-1, 1]^d$) trains Enc to group signals with similar patterns. As mentioned before, not only must healthy condition signals be grouped in one region in $\mathcal{F}$, but faulty condition signals should also be located in disjoint regions in $\mathcal{F}$ grouped by their class condition. This hypothesis will be experimentally tested in Section III.

Based on this assumption, a single representative vector, RV_k, of each class condition is obtained by applying Enc to each signal $s_k(t)$ of D_{shot}, i.e.,

$$RV_k = Enc(s_k(t)), \forall s_k(t) \in D_{shot} \tag{2}$$

The obtained RVs are the unique representatives of each condition in the feature space. Together, these vectors form the knowledge basis to perform the classification of previously unseen signals projected on $\mathcal{F}$. Moreover, since the computation of these vectors is independent of the mapping definition, retraining is not required, and thus the available knowledge can be incremented with signal projections under new conditions without affecting previously stored knowledge.

D. Fault diagnosis

In this last step, Enc is used to project a previously unseen signal s: $f = Enc(s)$, and then its class is obtained by comparing f with every RV obtained with Eq. 2.

The simplest way to perform this comparison is by means of any distance/norm in $\mathcal{F}$. Then, the estimated $\hat{c}$ condition of the new signal is assigned as the condition of the nearest representative:

$$\hat{c} = \underset{c \in C}{\operatorname{argmin}} \, ||RV_c - f|| \tag{3}$$

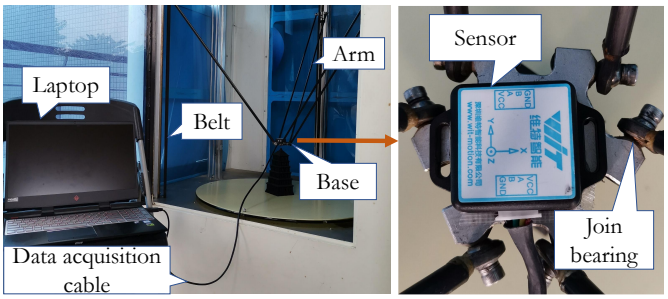

Fig. 3. 3D printer experimental setup.

This is a special case of the popular k-NN algorithm [39], with $k = 1$ and only one instance per class (RV_c).

III. Application and Results

In this section we present the test bed created for the acquisition of magnetic field signals in 3D printers for two failure modes, joint bearing and belt, with different locations for each of them. Then, the method presented in the previous section is applied to the 3D printer fault diagnosis, and compared with other unsupervised one-shot and supervised learning methods.

A. Delta 3D printer test bed

The experimental platform in Fig. 3 was used to collect data that served for the evaluation of the models. The 3D printer SLD-BL600-6 (SHILEIDI brand) consists mainly of a belt-driven mechanism of 3 degrees of freedom in delta type kinematic configuration, which is controlled by 3 bipolar stepper motors. The terminal points of each arm are coupled to the mobile elements employing joint bearings in order to have free rotational movement.

The magnetic field measurements were acquired with an AK8963 electronic compass integrated with a WIT MEMS BWT901 sensor. The resolution of this device was set to $14\,bits$, obtaining a sensitivity of $0.6\,uT$ in a total measurement range of $\pm 4900\,uT$. A frequency $f_s = 100\,samples/s$ was configured in this sensor, and the measured signals were sent to and stored in an Inspiron N4110 Laptop.

The eight evaluated conditions of the 3D printer are presented in Table I: one healthy condition (c_1), 3 fault mode locations by belt (c_2, c_3, c_4), and 4 fault modes by joint bearing ($c_5, ..., c_8$). The belt faults were simulated by decreasing the effective tension of each synchronous belt by $1.5\,mm$, and failures by joint bearing were created by unscrewing the corresponding clamping screw by 2 turns ($0.7\,mm$).

For each of these conditions, 20 circular patterns of $75\,mm$ radius each with a total duration of $324\,s$ were made by the head of the printer in the xy plane, and the magnetic field signals were stored during this time. This process was repeated 3 times, obtaining 3 signals of $32400\,samples$ length each. The first two signals were used to create the datasets D_{health} and D_{shot} used in our approach, and one more dataset D_{train} used for the comparison with supervised models. The third signal, in all cases, was used for building the D_{test} dataset

Fault code	Fault mode	Location
c_1 = H	-	-
c_2 = SB1	belt	axis 1
c_3 = SB2	belt	axis 2
c_4 = SB3	belt	axis 3
c_5 = JB1	joint bearing	arm 1, base end
c_6 = JB2	joint bearing	arm 2, base end
c_7 = JB3	joint bearing	arm 3, base end
c_8 = JB4	joint bearing	arm 1, carriage end

TABLE I
SIMULATED FAULTY CONDITIONS.

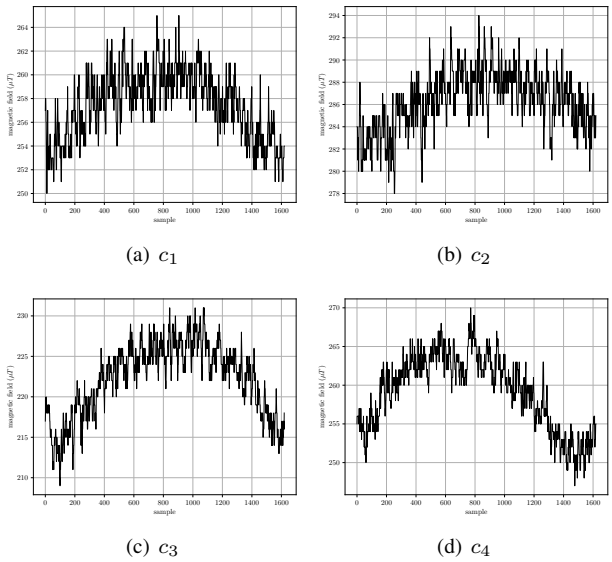

(a) c_1 (b) c_2 (c) c_3 (d) c_4

Fig. 4. Magnetic signals of healthy condition and fault in belts.

for evaluating the models' performance. In order to facilitate the evaluation process, we will take care that D_{test} is balanced, i.e., with an equal number of samples for every identified machine condition.

By sliding an extraction window over the original signal every 10 steps, 3078 sub-signals of length $T = 1620\,samples$ ($32400/20$), equivalent to the period required for one circle, were extracted from each acquired signal. This resulted in sizes of 49248 (6156 per condition), 6156 (only for c_1), 24624 (3078 per condition), and 8 (1 per condition) for D_{train}, D_{health}, D_{test}, and D_{shot}, respectively. Figures 4 and 5 show a chunk of these signals for the belt fault mode and joint bearing fault mode, respectively.

Table II shows details about the architectures of the neural networks for this study (for signals of length 1620, the optimal number of layers is 10). The Adam optimization algorithm [36] was set to values for learning rate, batch size, and number of epochs of 0.0002, 64 and 1000, respectively, for the three models.

B. Comparison with traditional methods

As previously mentioned, to our knowledge no other similar approaches in the field of fault diagnosis have been published for the solution of the problem addressed here. Therefore, it is not possible to provide a completely fair comparison with previous methods under the same conditions. However, the

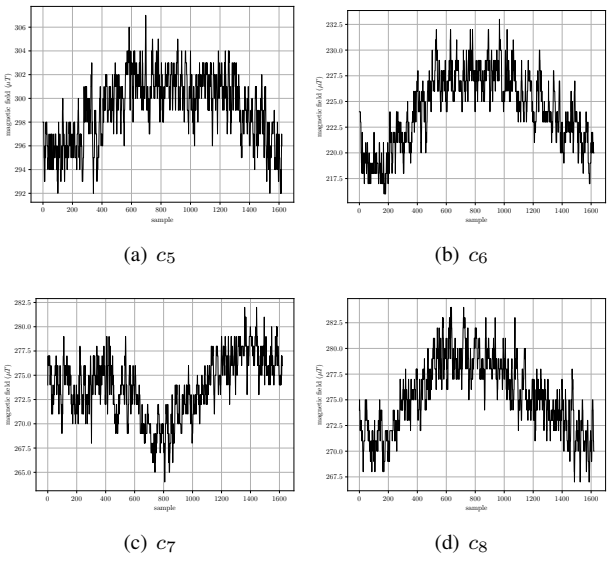

(a) c_5 (b) c_6 (c) c_7 (d) c_8

Fig. 5. Magnetic signals under faults in joint bearings.

Model	Parameter	Values									
Enc	layer	1	2	3	4	5	6	7	8	9	10
	kernel length	4	4	3	4	3	4	3	3	2	3
	output channels	2	4	8	16	32	64	128	256	512	100
	output length	810	405	202	101	50	25	12	6	3	1
	padding	no	no	yes	no	yes	no	yes	no	no	yes
	activation func.	LRL	LRL	LRL	LRL	LRL	LRL	LRL	LRL	LRL	LIN
Gen	layer	1	2	3	4	5	6	7	8	9	10
	kernel length	3	2	3	3	4	3	4	3	4	4
	output channels	512	256	128	64	32	16	8	4	2	1
	output length	3	6	12	25	50	101	202	405	810	1620
	padding	yes	no	no	yes	no	yes	no	yes	no	no
	activation func.	LRL	LRL	LRL	LRL	LRL	LRL	LRL	LRL	LRL	LIN
Dis	layer	1	2	3	4	5	6	7	8	9	10
	kernel length	4	4	3	4	3	4	3	3	2	3
	output channels	2	4	8	16	32	64	128	256	512	1
	output shape	810	405	202	101	50	25	12	5	3	1
	padding	no	no	yes	no	yes	no	yes	no	no	yes
	activation func.	LRL	LRL	LRL	LRL	LRL	LRL	LRL	LRL	LRL	LIN

TABLE II
ARCHITECTURE OF Enc, Gen AND Dis NETWORKS
(LRL = LEAKY-RELU, LIN = LINEAR)

core of the proposed method focuses on creating a useful embedding from the raw signal space into a feature space. Since this is also the aim of traditional approaches based on feature engineering, some kind of comparison is possible. The comparison is performed with the following methods:

1) One-Shot learning with expert Knowledge-based features (OS+EK): in this method, the feature space is obtained by previously reported expert knowledge. Therefore, the D_{health} dataset is not applicable, but steps 1, 3, and 4 are maintained with no modifications.
2) Random forest with expert Knowledge-based features (RF+EK): This approach follows the methodology reported in [15] for fault diagnosis model building. It uses features extracted with expert knowledge from D_{train} to train a random forest classifier. Hyperparameter optimization of this model is carried out using the grid search technique with the out-of-bag error as the performance metric. As we mentioned, real-world applications will not allow this data acquisition, but it is presented for comparative reasons.

		f-score			precision			recall		
Scenario	Cond.	**Prop.**	OS+EK	RF+EK	**Prop.**	OS+EK	RF+EK	**Prop.**	OS+EK	RF+EK
Belt	H	100.0	87.79	100.0	100.0	92.67	100.0	100.0	83.40	100.0
	SB1	100.0	88.95	100.0	100.0	84.91	100.0	100.0	93.41	100.0
	SB2	100.0	100.0	66.67	100.0	100.0	50.0	100.0	100.0	100.0
	SB3	100.0	100.0	0.0	100.0	100.0	0.0	100.0	100.0	0.0
Joint bearing	H	99.74	78.86	99.97	99.48	87.27	100.0	100.0	71.93	99.94
	JB1	100.0	83.25	100.0	100.0	87.62	100.0	100.0	79.31	100.00
	JB2	98.56	99.18	98.34	97.16	99.97	96.73	100.0	98.41	100.0
	JB3	100.0	99.95	98.25	100.0	99.90	99.93	100.0	100.0	96.62
	JB4	98.25	70.40	100.0	100.0	62.59	100.0	96.56	80.44	100.0
Combined	H	99.74	77.37	100.0	99.48	83.71	100.0	100.0	71.93	100.0
	JB1	100.0	59.96	100.0	100.0	85.41	100.0	100.0	46.20	100.0
	JB2	98.56	86.99	98.07	97.16	78.02	96.22	100.0	98.28	100.0
	JB3	99.97	95.33	73.67	99.94	98.41	59.75	100.0	92.43	96.07
	JB4	98.20	69.71	100.0	99.90	68.54	100.0	96.56	70.92	100.0
	SB1	99.95	63.88	100.0	100.0	52.16	100.0	99.90	82.39	100.0
	SB2	100.0	83.80	85.01	100.0	99.55	73.93	100.0	72.35	100.0
	SB3	99.97	95.68	0.0	100.0	92.98	0.0	99.94	98.54	0.0

TABLE III
DIAGNOSIS RESULTS OF COMPARED METHODS
(PROP. IS THE METHOD PROPOSED HERE)

It must be noted that other comparisons with supervised fault diagnosis approaches do not contribute to the evaluation of the proposal, and, consequently, they are beyond the scope of this work.

Two important points need to be made: (i) the input of our method is the raw magnetic field signal without preprocessing or feature extraction, and (ii) OS+EK and RF+EK have the same expert knowledge-based features (EK features). These EK features are the scalars: crest factor, shape factor, absolute mean amplitude, square root amplitude, kurtosis, variance value, clearance factor, impulse indicator, and skewness factor. Specifically, the feature vector for each signal is created by the following (details can be found in [40]):

1) Calculate the 9 EK features of the signal in the time domain.
2) Calculate the 9 EK features of the signal in the frequency domain.
3) Decompose the signal in 32 time–frequency coefficients through wavelet packet transform (5 levels) and calculate the 9 EK features of each coefficient.
4) Group previous features into a 306-length vector (9 time + 9 frequency + 9×32 time-frequency).

Thus, for OS+EK, the RVs are the feature vectors computed with signals from D_{shot}; meanwhile, for RF+EK, the classifier is created through the feature vectors computed with signals from D_{train}.

For each scenario (failure in belts, failures in joint bearings, and the combination of these two scenarios), 20 trials of diagnosing with the D_{test} dataset were performed and compared, all of them containing the healthy condition. Table III summarizes the diagnosis results for each scenario and method averaged over these trials, and Table IV shows confusion matrices for each fault condition and method in the combined scenario (the most challenging).

F-score, precision, and recall were 100% in the diagnosis of belt faults when applying our proposal. However, in the case of joint bearing failures, some examples from JB4 were classified as JB2 and some even as H. The JB4 condition has the worst recall (96.56%) and JB2 the worst precision (97.16%) for the

Model	R/P	H	JB1	JB2	JB3	JB4	SB1	SB2	SB3
Prop.	H	3078	0	0	0	0	0	0	0
	JB1	0	3078	0	0	0	0	0	0
	JB2	0	0	3078	0	0	0	0	0
	JB3	0	0	0	3078	0	0	0	0
	JB4	16	0	90	0	2972	0	0	0
	SB1	0	0	0	0	3	3075	0	0
	SB2	0	0	0	0	0	0	3078	0
	SB3	0	0	0	2	0	0	0	3076
OS+EK	H	2214	1	1	0	575	287	0	0
	JB1	0	1422	0	0	64	1592	0	0
	JB2	46	0	3025	1	0	0	6	0
	JB3	0	0	0	2845	0	0	4	229
	JB4	277	171	0	0	2183	447	0	0
	SB1	108	71	0	0	363	2536	0	0
	SB2	0	0	851	0	0	0	2227	0
	SB3	0	0	0	45	0	0	0	3033
RF+EK	H	3079	0	0	0	0	0	0	0
	JB1	0	3079	0	0	0	0	0	0
	JB2	0	0	3079	0	0	0	0	0
	JB3	0	0	121	2958	0	0	0	0
	JB4	0	0	0	0	3079	0	0	0
	SB1	0	0	0	0	0	3079	0	0
	SB2	0	0	0	0	0	0	3079	0
	SB3	0	0	0	1993	0	0	1086	0

TABLE IV
CONFUSION MATRICES IN THE COMBINED CASE

combined case. The 90 examples of JB4 that are misclassified as JB2 are the main reason for a precision loss in JB2.

In belt faults, the OS+EK method has decrements in precision and recall in the healthy condition. The former is explained by the decrease in recall in SB1, showing that instances from SB1 were misclassified as healthy. The decrease in recall shows that instances from H were misclassified as SB1. In joint bearings, this method presents the worst performance with a minimum f-score of 70.4% for JB4. In the combined case, the worst recall (46.20%) can be seen in JB1 and the worst precision (52.16%) in SB1. This can be explained by the 1592 examples of JB1 that are misclassified as SB1.

The results for RF+EK show that the model misclassified all instances from SB3 as SB2 in the belt faults case. In the joint bearings case, examples from JB3 are confused with those from JB2, and some examples from H are confused with those from JB3. In the combined case, the worst precision and recall are obtained in SB3, as in the first case. The loss of precision and recall in SB3 is because all examples from this condition are misclassified in SB2 and JB3. This differs from the first case where the loss of these metrics was due only to instances classified in SB2. These findings suggest that JB3 must occupy a zone close to SB2 in the expert-Knowledge feature space.

C. Comparison with other deep learning methods

It is necessary to compare our proposal with other state-of-the-art methods focused on the unsupervised feature extraction task. DCAE, CDBN, and ESN-VAE were selected for this purpose, all using raw magnetic field signals as input and trained with the D_{health} dataset. More details about DCAE, CDBN and ESN-VAE architecture and optimization can be seen in [22], [23], and [26], respectively. To allow a comparison, after feature learning with these methods, step 3 of our proposal will produce RVs, and step 4 will perform the diagnosis over D_{test}.

Figure 6(f) shows the results of these DL methods in the three scenarios and compares them to the results obtained by the proposed method. Although all of the DL methods outperform OS+EK, and ESN-VAE surpasses RF+EK in the combined case, their performances are far behind the performance of our method. Notice also that the other DL methods have reported state-of-the-art results extracting features using examples from all of the machinery conditions, but they have not been tested using examples in the healthy condition only. Our proposal shows a performance at least as good as RF+EK (supervised approach with data from all of the conditions) for the fault diagnosis in joint bearings (99.31%), and considerably higher performance (100% and 99.95%) in the other two cases. Furthermore, our proposal is not affected by the increase in the number of conditions as the accuracy for belt and joint bearing cases with 4 classes are 100% and 99.31%, respectively, and is 99.55% for the combined case with 8 classes. In contrast, OS+EK shows a lower performance when faced with a larger number of conditions.

All of these considerations show that instances from new conditions occupy sufficiently separated zones in the feature space. Figures 6(a)–6(e) compare the feature spaces through a 2D projection of the instances in D_{test} using the t-SNE algorithm [41], which projects the points from a high-dimensional space (306 dimensions for EK features, 100 dimensions for the others) to a 2D space. The high complexity that the classifier has to deal with in order to separate the conditions in the feature spaces of the different methods is remarkable. Specifically, examples from the SB3 condition appear widely scattered in all other models, making it difficult to classify them correctly. However, this is not the case in our proposal, where a correct grouping and separation of the instances of all the 3D printer conditions can be observed. Undoubtedly, these observations experimentally prove the hypothesis proposed in Section II-C.

D. Sensibility and detectability tests

The sensibility of the proposed method on the D_{health} set size in the combined case has also been evaluated. Figure 7 shows the average accuracy performance on D_{test} and the 95% confidence interval using the models obtained by using 10% (616) to 100% (6156) of the samples from D_{health} (in steps of 10%). Twenty trials were performed by randomly selecting the elements from D_{train} and D_{shot} in order to reduce the bias caused by different network initialization and elements in D_{shot}. As expected, performance increases with training set size, and it only requires 60% (3694 examples) of the training data to overcome the other traditional and DL approaches with an accuracy of $92.07\% \pm 1.24$.

With our method, signals from a totally new faulty condition will be classified as the condition of the closest RV. However, it would be more interesting to recognize if they do not belong to any of the currently known conditions. To include an approximation of this feature in our proposal, let d^c_{nrt} and d^c_{avg} be the minimum and average distances, respectively, from a current condition set of signals to the centroid of some known

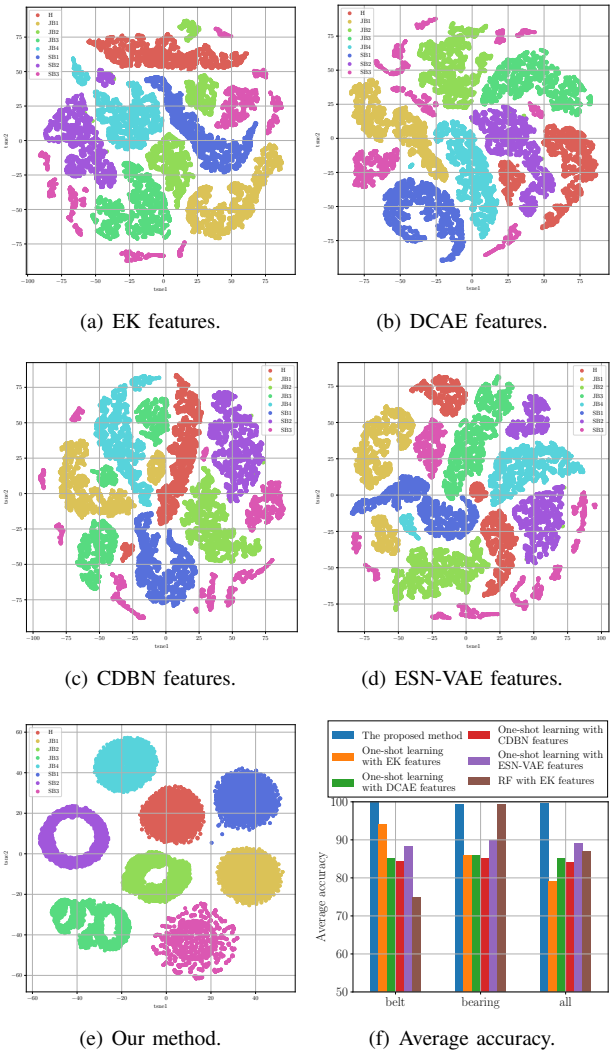

(a) EK features. (b) DCAE features. (c) CDBN features. (d) ESN-VAE features. (e) Our method. (f) Average accuracy.

Fig. 6. (a-e) 2D projections using t-SNE, and (f) overall comparison.

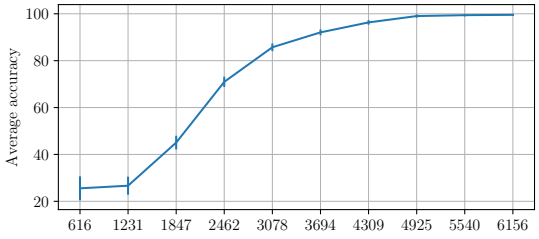

Fig. 7. Diagnosis performance under different training set sizes.

condition cluster, c. We also let d^c_{far} be the maximum distance between the samples in c to its centroid. Then, the ratios

$$r^c_{avg} = \frac{d^c_{avg}}{d^c_{far}}, \qquad r^c_{nrt} = \frac{d^c_{nrt}}{d^c_{far}}, \tag{4}$$

report the average and worst undetectabilities, respectively. We can use the protocol of classifying the current condition as c when $r^c_{nrt} \leq 1$.

Table V summarizes the detection ability of this new protocol in each available fault condition. Although most of the faults can be detected as different conditions, two mistakes are observed: JB3 detected as SB3, and SB2 detected as JB3. However, it is important to stress that these ratios show extreme conditions, and in practical cases it will be fulfilled only when (i) the RV of the known condition is the farthest point of its cluster, and (ii) the new sample is the closest point to the centroid of the known condition cluster. Meeting both conditions is not easy, and therefore the probability of mistake is reduced in real-world cases.

Unseen faults	Known condition clusters															
	H		JB1		JB2		JB3		JB4		SB1		SB2		SB3	
	r_{nrt}	r_{avg}	r_{nrt}	r_{avg}	r_{nrt}	r_{avg}	r_{nrt}	r_{avg}	r_{nrt}	r_{avg}	r_{nrt}	r_{avg}	r_{nrt}	r_{avg}	r_{nrt}	r_{avg}
JB1	13.16	14.19	-	-	10.02	10.87	2.13	2.31	3.00	3.37	1.55	1.92	8.13	8.86	2.25	2.46
JB2	2.44	2.97	3.83	3.96	-	-	1.01	1.14	1.56	1.67	3.01	3.16	1.06	1.51	1.86	2.00
JB3	6.88	7.94	3.15	3.26	3.50	4.41	-	-	1.95	2.21	2.66	2.74	1.76	2.53	0.58	0.73
JB4	4.68	5.62	2.51	2.81	3.43	4.08	1.20	1.35	-	-	1.43	1.77	3.08	3.58	1.84	2.04
SB1	8.79	9.64	1.25	1.55	6.41	7.14	1.46	1.61	1.37	1.71	-	-	5.15	5.77	1.79	1.98
SB2	4.35	4.75	3.55	3.66	1.41	1.77	0.66	0.76	1.60	1.67	2.78	2.89	-	-	1.45	1.56
SB3	9.72	11.11	2.94	3.16	6.06	7.16	2.15	2.62	2.73	3.13	2.85	3.12	4.11	4.98	-	-

TABLE V
UNDETECTABILITY RATIOS UNDER UNSEEN FAULT CONDITIONS.

IV. CONCLUSIONS

In this work, a new one-shot learning-based method has been proposed for fault diagnosis in industrial devices when a large amount of signals from some healthy conditions and only one signal from some of the fault conditions are available. In our methodology, a first step of signal acquisition is required considering the real conditions of data availability, where signals in the healthy condition are available in abundance in the initial current lifetime of the machine. Next, a mapping function is obtained that transforms signals under an unknown probability distribution into vectors of a feature space under a known uniform distribution. This mapping is learned from signals in the healthy condition only by using a BiGAN-based approach. Representatives of the classification regions of each health condition are then obtained by mapping fault condition signals (usually only one, thus achieving the one-shot learning) into the feature space. Finally, condition classification of a new signal is determined by measuring the distances between the mapping of the signal to the precomputed RVs.

The proposed approach has been applied in 3 cases of fault diagnosis in 3D printers: 3 failures in belts, 4 failures in joint bearings, and the combination of these failures (7 failures plus the healthy condition). The resulting model was able to correctly diagnose these 3D printer conditions from signals acquired with a magnetic field sensor. For comparative purposes, other methods from the literature have also been applied to the same case studies, and the results allow us to make the following statements:

1) Magnetic field signals contain information useful for the fault diagnosis in 3D printers. These signals could be an alternative to the use of vibration and acoustic emission signals, resulting in a considerable reduction in the cost of diagnostic systems.
2) Signals in the healthy condition provides enough information to create a mapping to a suitable feature space under an unsupervised approach. Only one signal in every fault condition is required to separate classification regions in this space.

3) Our method needs far fewer examples for the construction of this mapping (only 60% of those needed for other methods using DL techniques).
4) We have also provided a mechanism (only a first and simple protocol has been presented here) to recognize when a new sample should not be classified as any of the current known conditions (healthy or not).

REFERENCES

[1] C. Balletti, M. Ballarin, and F. Guerra, "3d printing: State of the art and future perspectives," *Journal of Cultural Heritage*, vol. 26, DOI 10.1016/j.culher.2017.02.010, pp. 172–182, Jul. 2017.

[2] T. Sathish, M. Vijayakumar, and A. K. Ayyangar, "Design and fabrication of industrial components using 3d printing," *Materials Today: Proceedings*, vol. 5, DOI 10.1016/j.matpr.2018.03.036, no. 6, pp. 14 489–14 498, 2018.

[3] M. Yampolskiy, A. Skjellum, M. Kretzschmar, R. A. Overfelt, K. R. Sloan, and A. Yasinsac, "Using 3d printers as weapons," *International Journal of Critical Infrastructure Protection*, vol. 14, DOI 10.1016/j.ijcip.2015.12.004, pp. 58–71, Sep. 2016.

[4] T. D. Ngo, A. Kashani, G. Imbalzano, K. T. Nguyen, and D. Hui, "Additive manufacturing (3d printing): A review of materials, methods, applications and challenges," *Composites Part B: Engineering*, vol. 143, DOI 10.1016/j.compositesb.2018.02.012, pp. 172–196, Jun. 2018.

[5] J. Long, S. Zhang, and C. Li, "Evolving deep echo state networks for intelligent fault diagnosis," *IEEE Transactions on Industrial Informatics*, vol. 16, DOI 10.1109/tii.2019.2938884, no. 7, pp. 4928–4937, Jul. 2020. [Online]. Available: https://doi.org/10.1109/tii.2019.2938884

[6] A. Khadersab and S. Shivakumar, "Parametric vibration analysis of rotating machinery," *Materials Today: Proceedings*, vol. 5, DOI 10.1016/j.matpr.2018.11.010, no. 11, pp. 25 688–25 696, 2018.

[7] C. Li, R.-V. Sanchez, G. Zurita, M. Cerrada, D. Cabrera, and R. E. Vásquez, "Gearbox fault diagnosis based on deep random forest fusion of acoustic and vibratory signals," *Mechanical Systems and Signal Processing*, vol. 76-77, DOI 10.1016/j.ymssp.2016.02.007, pp. 283–293, Aug. 2016.

[8] Y. Lu and Y. Wang, "Monitoring temperature in additive manufacturing with physics-based compressive sensing," *Journal of Manufacturing Systems*, vol. 48, DOI 10.1016/j.jmsy.2018.05.010, pp. 60–70, Jul. 2018.

[9] K. He, Z. Yang, Y. Bai, J. Long, and C. Li, "Intelligent fault diagnosis of delta 3d printers using attitude sensors based on support vector machines," *Sensors*, vol. 18, DOI 10.3390/s18041298, no. 4, p. 1298, Apr. 2018.

[10] Z. Qiao, Y. Lei, and N. Li, "Applications of stochastic resonance to machinery fault detection: A review and tutorial," *Mechanical Systems and Signal Processing*, vol. 122, DOI 10.1016/j.ymssp.2018.12.032, pp. 502–536, May. 2019.

[11] Z. Li and B. Shi, "A piecewise nonlinear stochastic resonance method and its application to incipient fault diagnosis of machinery," *Chinese Journal of Physics*, vol. 59, DOI 10.1016/j.cjph.2019.02.026, pp. 126–137, Jun. 2019.

[12] X. Zhang, J. Wang, Z. Liu, and J. Wang, "Weak feature enhancement in machinery fault diagnosis using empirical wavelet transform and an improved adaptive bistable stochastic resonance," *ISA Transactions*, vol. 84, DOI 10.1016/j.isatra.2018.09.022, pp. 283–295, Jan. 2019.

[13] C. Li, J. L. V. de Oliveira, M. C. Lozada, D. Cabrera, V. Sanchez, and G. Zurita, "A systematic review of fuzzy formalisms for bearing fault diagnosis," *IEEE Transactions on Fuzzy Systems*, DOI 10.1109/tfuzz.2018.2878200, pp. 1–1, 2018. [Online]. Available: https://doi.org/10.1109/tfuzz.2018.2878200

[14] C. Li, M. Cerrada, D. Cabrera, R. V. Sanchez, F. Pacheco, G. Ulutagay, and J. V. de Oliveira, "A comparison of fuzzy clustering algorithms for bearing fault diagnosis," *Journal of Intelligent & Fuzzy Systems*, vol. 34, DOI 10.3233/JIFS-169534, no. 6, p. 3565–3580, Jun. 2018. [Online]. Available: http://doi.org/10.3233/JIFS-169534

[15] D. Cabrera, F. Sancho, R.-V. Sánchez, G. Zurita, M. Cerrada, C. Li, and R. E. Vásquez, "Fault diagnosis of spur gearbox based on random forest and wavelet packet decomposition," *Frontiers of Mechanical Engineering*, vol. 10, DOI 10.1007/s11465-015-0348-8, no. 3, pp. 277–286, Sep. 2015.

[16] M. Cerrada, G. Zurita, D. Cabrera, R.-V. Sánchez, M. Artés, and C. Li, "Fault diagnosis in spur gears based on genetic algorithm and random forest," *Mechanical Systems and Signal Processing*, vol. 70-71, DOI 10.1016/j.ymssp.2015.08.030, pp. 87–103, Mar. 2016.

[17] J. K. Yoon, D. He, and B. V. Hecke, "A phm approach to additive manufacturing equipment health monitoring, fault diagnosis, and quality control," 2014.

[18] M. Cerrada, R.-V. Sánchez, F. Pacheco, D. Cabrera, G. Zurita, and C. Li, "Hierarchical feature selection based on relative dependency for gear fault diagnosis," *Applied Intelligence*, vol. 44, no. 3, pp. 687–703, 2016.

[19] F. Pacheco, M. Cerrada, R.-V. Sánchez, D. Cabrera, C. Li, and J. V. de Oliveira, "Attribute clustering using rough set theory for feature selection in fault severity classification of rotating machinery," *Expert Systems with Applications*, vol. 71, pp. 69 – 86, 2017.

[20] S. Zhang, S. Zhang, B. Wang, and T. G. Habetler, "Machine learning and deep learning algorithms for bearing fault diagnostics – a comprehensive review," *arXiv:1901.08247v2*, 2019.

[21] J. Long, Z. Sun, C. Li, Y. Hong, Y. Bai, and S. Zhang, "A novel sparse echo autoencoder network for data-driven fault diagnosis of delta 3-d printers," *IEEE Transactions on Instrumentation and Measurement*, DOI 10.1109/tim.2019.2905752, pp. 1–10, 2019.

[22] D. Cabrera, F. Sancho, C. Li, M. Cerrada, R.-V. Sánchez, F. Pacheco, and J. V. de Oliveira, "Automatic feature extraction of time-series applied to fault severity assessment of helical gearbox in stationary and non-stationary speed operation," *Applied Soft Computing*, vol. 58, DOI 10.1016/j.asoc.2017.04.016, pp. 53–64, Sep. 2017. [Online]. Available: https://doi.org/10.1016/j.asoc.2017.04.016

[23] H. Shao, H. Jiang, H. Zhang, and T. Liang, "Electric locomotive bearing fault diagnosis using a novel convolutional deep belief network," *IEEE Transactions on Industrial Electronics*, vol. 65, DOI 10.1109/tie.2017.2745473, no. 3, pp. 2727–2736, Mar. 2018.

[24] J. Guo, J. Wu, Z. Sun, J. Long, and S. Zhang, "Fault diagnosis of delta 3d printers using transfer support vector machine with attitude signals," *IEEE Access*, vol. 7, DOI 10.1109/access.2019.2905264, pp. 40 359–40 368, 2019.

[25] S. Zhang, Z. Sun, J. Long, C. Li, and Y. Bai, "Dynamic condition monitoring for 3d printers by using error fusion of multiple sparse auto-encoders," *Computers in Industry*, vol. 105, DOI 10.1016/j.compind.2018.12.004, pp. 164–176, Feb. 2019.

[26] D. Cabrera, F. Sancho, M. Cerrada, R.-V. Sánchez, and F. Tobar, "Echo state network and variational autoencoder for efficient one-class learning on dynamical systems," *Journal of Intelligent & Fuzzy Systems*, vol. 34, DOI 10.3233/JIFS-169552, no. 6, p. 3799–3809, Jun. 2018. [Online]. Available: http://doi.org/10.3233/JIFS-169552

[27] S. Plakias and Y. S. Boutalis, "Exploiting the generative adversarial framework for one-class multi-dimensional fault detection," *Neurocomputing*, vol. 332, DOI 10.1016/j.neucom.2018.12.041, pp. 396–405, Mar. 2019.

[28] H. Liu, J. Zhou, Y. Xu, Y. Zheng, X. Peng, and W. Jiang, "Unsupervised fault diagnosis of rolling bearings using a deep neural network based on generative adversarial networks," *Neurocomputing*, vol. 315, DOI 10.1016/j.neucom.2018.07.034, pp. 412–424, Nov. 2018.

[29] L. Fei-fei, "Knowledge transfer in learning to recognize visual object classes," in *In: International Conference on Development and Learning (ICDL*, 2006.

[30] M. Rodriguez, C. Orrite, C. Medrano, and D. Makris, "One-shot learning of human activity with an MAP adapted GMM and simplex-HMM," *IEEE Transactions on Cybernetics*, vol. 47, DOI 10.1109/tcyb.2016.2558447, no. 7, pp. 1769–1780, Jul. 2017.

[31] H. Sun, Y. Xiao, J. Wang, J. Wang, Q. Qi, J. Liao, and X. Liu, "Common knowledge based and one-shot learning enabled multi-task traffic classification," *IEEE Access*, vol. 7, DOI 10.1109/access.2019.2904039, pp. 39 485–39 495, 2019.

[32] J. Weis and A. Santra, "One-shot learning for robust material classification using millimeter-wave radar system," *IEEE Sensors Letters*, vol. 2, DOI 10.1109/lsens.2018.2878041, no. 4, pp. 1–4, Dec. 2018.

[33] A. Zhang, S. Li, Y. Cui, W. Yang, R. Dong, and J. Hu, "Limited data rolling bearing fault diagnosis with few-shot learning," *IEEE Access*, DOI 10.1109/access.2019.2934233, pp. 1–1, 2019.

[34] L. Devroye, *Non-Uniform Random Variate Generation(originally published with*. Springer-Verlag, 1986. [Online]. Available: http://cg.scs.carleton.ca/~luc/rnbookindex.html

[35] J. Donahue, P. Krähenbühl, and T. Darrell, "Adversarial feature learning."

[36] D. P. Kingma and J. Ba, "Adam: A method for stochastic optimization," *arXiv:1412.6980v9*, 2014.

[37] S. Ioffe and C. Szegedy, "Batch normalization: Accelerating deep network training by reducing internal covariate shift."

[38] V. Dumoulin and F. Visin, "A guide to convolution arithmetic for deep learning," *arXiv:1603.07285v2*, 2018.

[39] N. S. Altman, "An introduction to kernel and nearest-neighbor nonparametric regression," *The American Statistician*, vol. 46, DOI 10.1080/00031305.1992.10475879, no. 3, pp. 175–185, Aug. 1992.

[40] C. Li, R.-V. Sanchez, G. Zurita, M. Cerrada, D. Cabrera, and R. E. Vásquez, "Multimodal deep support vector classification with homologous features and its application to gearbox fault diagnosis," *Neurocomputing*, vol. 168, DOI 10.1016/j.neucom.2015.06.008, pp. 119–127, Nov. 2015.

[41] L. van der Maaten and G. Hinton, "Visualizing data using t-SNE," *Journal of Machine Learning Research*, vol. 9, pp. 2579–2605, 2008. [Online]. Available: http://www.jmlr.org/papers/v9/vandermaaten08a.html